Role of *in situ* (in contact with biomass) and *ex situ* (in contact with pyrolysis vapors) transition metal catalysts on pyrolysis of cherry pits

Andrew H. Hubble[a], Bridget A. Childs[a], Matteo Pecchi[a], Hanifrahmawan Sudibyo[b], Jefferson W. Tester[b], Jillian L. Goldfarb[a]*

[a] Department of Biological & Environmental Engineering, Cornell University, Ithaca NY 14853, USA
[b] Smith School of Chemical & Biomolecular Engineering, Cornell University, Ithaca NY 14853, USA

Prepared for Submission to: *Fuel*

Abstract

While energy dense liquid biofuels can be produced from sustainable waste feedstocks via thermochemical conversion techniques, these biofuels are plagued by high acidity and low stability, largely due to the presence of oxygenated functional groups. By utilizing transition metal catalysts during pyrolysis either *in situ* within the biomass, or *ex situ* (directly downstream supported on an alumina substrate) acting on the pyrolysis vapors, the quality of the bio-oil can be improved via deoxygenation. Four transition metals (Cu, Mn, Ni, Zn) were either wet impregnated on cherry pit biomass, or by impregnated on alumina wool fibers placed downstream of the biomass to act on the devolatilized gases. The *in situ* catalysts Cu, Mn and Zn increase the pyrolysis bio-oil yield. The Mn, Ni and Zn used as *ex situ* catalysts increase the total non-condensable gas produced, suggesting that these downstream catalysts crack the pyrolyzed molecules into smaller organics and water. The *ex situ* catalysts result in larger quantities of especially oxygen-containing gases like CO_2, which in turn lowered the bio-oil's O/C ratio. However, such reactions also increase the water content of the resulting bio-oil. Both Mn and Zn used in either location enhance the concentration of alcohols relative to aromatic carbons, and when used *ex situ*, Mn shows a decrease in the ratio of aromatic to aliphatic carbon content.

Keywords: Pyrolysis, Catalysts, Transition metals, Cherry pits, Bio-oil

* To whom correspondence should be addressed: goldfarb@cornell.edu, 607.255.5789

1. Introduction

The widespread adoption of liquid biofuels is critical for climate change mitigation in sectors that require high-density combustible liquid fuels for the foreseeable future [1]. In September 2021, the Biden administration set a production goal of three billion gallons of sustainable aviation fuel by 2030, and a completely carbon neutral aviation sector by 2050 [2]. Using liquid biofuels from pyrolysis of lignocellulosic feedstocks in the current fossil fuel infrastructure is hindered by complex and costly upgrading of as-produced bio-oils. One of the largest inhibiting factors of pyrolysis bio-oil utilization is its high oxygen content [3,4] which increases fuel acidity [5] and viscosity [6] (further increasing viscosity during storage [7]), and lowers energy density [8,9]. Pyrolysis bio-oils are upgraded via multiple unit operations, including distillation [10], steam reformation [11] and hydrodeoxygenation [12]. However, the cost of cascading numerous upgrading processes limits the economic viability of biomass to biofuel conversions. Instead, *in situ* catalytic upgrading has gained traction over the years, whereby the catalyst and feedstock are co-mingled into a single-step thermochemical conversion to reduce the need for intensive downstream upgrading [13–15].

A growing body of literature explores the use of transition metals (TMs) [16–18] as inexpensive alternatives to precious metal catalysts such as platinum-group metals [19–21]. TMs are often scaffolded onto frameworks like zeolites. For example, Dyer et al. examined the effects of zeolite-metal catalysts on bio-oil and gas composition of co-pyrolyzed biomass-polystyrene [22], and Li et al. paired transition metals with zeolites to improve the hydrodeoxygenation (HDO) of guaiacol [23]. Copper-zeolite catalysts can achieve upwards of 96% conversion of glucose to hydroxymethylfurfural, and 92% of xylose could be converted to furfural over a copper-

mesoporous silica catalyst [24]. While these and other works show improved yields and identify key mechanisms for various pyrolytic biomass transformations, there is little discussion in the literature about the combined effects of the TM-scaffold catalysts' components.

In addition to bespoke TM-scaffold catalysts, naturally occurring heterogeneous catalysts (such as clay minerals) and process wastes (e.g. spent drilling mud and adsorbents) that contain TMs are often used to upgrade pyrolysis bio-oils either *in situ* or downstream. For example, Chen et al. demonstrated how copper slag can accelerate the devolatilization of sewage sludge [25]. Our group previously demonstrated how *in situ* addition of clays such as montmorillonite can enhance deoxygenation reactions, whereas attapulgite increases alkylation, ketonization, and aldol condensation reactions [26]. While important additions to the field, many of these works cannot speak to the impact of the TM contained within the clay or waste on the pyrolysis reactions. Recently, Praserttaweepron et al. demonstrated how Ni-doping of dolomite clay promoted decarboxylation, decarbonylation and secondary tar cracking reactions to enhance hydrocarbon yields [27]. As the Ni concentration increased, the non-condensable gas yield increased. As there was no Ni-only run performed, we cannot determine if this effect is due only to the presence of Ni, or synergistic effects between the Ni and dolomite. Similarly, TMs supported on activated biochar (AB) show greater deoxygenation potential than alkali metal oxides on biochar [28]. However, as ABs themselves show catalytic activity during biomass pyrolysis [29], the TM-AB complex may be responsible for the deoxygenation, rather than the TM itself. Synergistic effects between co-catalysts exist across many areas of catalysis, from dichloromethane oxidation [30], to base-free oxidation of glycerol [31], to hydrogen production

by steam reforming of ethanol [32]. As such, one goal of this paper is to understand the potential role of single TMs in biomass pyrolysis by decoupling the TM and scaffold/mixture effects.

TM pyrolysis catalyst studies in the literature often investigate specific compound and conversion pathways rather than actual mixtures of biomass pyrolysis products. For example, Resasco et al. used platinum to upgrade m-cresol, an important bio-oil component and intermediary, but one that is not necessarily representative of heterogeneous pyrolysis bio-oils [33]. Bodachivskyi et al. started with the representative biomass feedstock (cellulose) and tracked ethyl levulinate production over metal triflate catalysts. While achieving yields and selectivity of over 70% and 80% respectively [34], pyrolysis of heterogeneous biomass generates hundreds of compounds [6,35] of which ethyl levulinate represents but one potential mixture component. The effects of the transition metals on "real" (heterogeneous) biomass thermochemical conversions are a nascent area of research.

During pyrolysis, a TM catalyst could act on vapor phase reactions (i.e. devolatilized gases), and (or) on reactions at the solid-vapor interface (i.e. devolatilization, primary decomposition, or the formation of biochar). Recondensation at the solid-vapor phase boundary causes (re)deposition of tar onto the biochar, which alters biochar yield, quality and potential further pyrolytic reactions, whereas tar-forming compounds that enter the pyrolysis vapor phase could drastically alter the composition of the bio-oil once it condenses [36]. A catalyst placed *in situ* – that is, within the pyrolyzing biomass – could impact both interfacial and vapor phase reactions.

A catalyst placed downstream of the devolatilization zone (termed here *ex situ* catalysis) will only contact the devolatilized gases.[1] The catalyst position can lead to vastly different bio-oil compound distributions, depending on the feedstocks. For example, the concentration of fatty acids in pyrolysis bio-oil were halved when CaO was used as a downstream catalyst versus *in situ* positioning [37], likely due to decarboxylation and decarbonylation reactions in the vapor phase. A commercial HZSM-5 zeolite was used by Wang et al. to study the catalytic pyrolysis of hybrid poplar. In this instance, *in situ* pyrolysis yield more aromatic compounds, whereas *ex situ* saw three times as many olefins; aromatics that did form from *ex situ* pyrolysis were predominantly monocyclic aromatics, whereas *in situ* favored polycyclic aromatics [38].

Iisa et al. made a compelling techno-economic argument that partial deoxygenation via *ex situ* upgrading could mitigate bio-oil instability, which would facilitate transportation and produce a distillable bio-oil. In turn, this would reduce hydrogen requirements (and therefore costs) for downstream hydrotreating [39]. As such, a second goal of this work is to explore the impact of TMs on deoxygenation when placed in contact with biomass (*in situ*) and in contact with uncondensed pyrolysis vapors (*ex situ*).

2. Materials and methods

Cherry pits were used as a model biomass feedstock given their reasonably uniform composition [40–42] and large untapped potential resource with nearly four million tons produced globally in 2020 [43]. In the U.S. cherry pit production reached 400,000 tons annually (2020) [44] with the

[1] We note that *ex situ* pyrolysis is also used to describe downstream upgrading of condensed pyrolysis vapors in a separate unit operation. Such a definition is used in the review of *in situ* versus *ex situ* deoxygenation of pyrolysis products by Saraeian et al. [72]. The exploration of TM on this form of *ex situ* upgrading is beyond the scope of this work.

majority processed by a single facility in the Great Lakes region, concentrating the cherry pits in one location [42]. American tart cherry pits (*prunus cerasus*) were supplied by the Great Lakes Packing Company in Kewadin, MI, where they are dried onsite at 120 °C for one hour and stored in bulk in grain silos. Upon arrival at Cornell University, the cherry pits were washed with deionized water, dried at room temperature, and ground and sieved to 1-2 mm (with brass ASTM sieves). While it would be somewhat impractical to wash dry biomass prior to pyrolysis, samples were washed to ensure samples were as homogeneous as possible to enhance reproducibility. From prior work with this feedstock, the cherry pits contain between 77.7 – 80.7 wt% volatile matter, 16.0 - 22.3 wt% fixed carbon and 0 – 3.3 wt% non-oxidizable inorganic matter [42].

2.1 Catalyst preparation

Four metal acetate compounds were sourced from Sigma Aldrich: copper(II) [Cat:341746, 98%], manganese(II) [Cat:221007, ≥99%], nickel(II) [Cat:244066, 98%], and zinc [Cat:383058, ≥98%] and were used as received. A wet impregnation method, similar to those detailed by Haukka et al. and Sietsma et al. [45,46], was used for this work.

For the *in situ* experiments, biomass was directly contacted with the TMs. 0.05 M solutions of each metal acetate were prepared using Milli-Q water (18.2 mq·cm/25 °C). Six grams of cherry pits were soaked in 50.0 mL of each metal acetate solution for one hour. After this soak time, the samples were vacuum filtered through a Buchner funnel over cellulose filter paper (Whatman, 47 μm). The filtered samples were dried at ambient conditions for 48 hours. As an experimental control for *in situ* experiments, and to provide biomass samples for *ex situ* experiments, cherry pits were soaked in pure Milli-q water in the same 6 g: 50 mL water ratio, then filtered and dried.

To synthesize the *ex situ* catalysts, 0.3 grams of alumina oxide wool fibers (Merck 142844-00-6) were soaked in 50 mL of the 0.05 M metal acetate solutions for one hour. The alumina fibers were removed from the soak solution using tweezers and dried at ambient conditions for 48 hours. This quantity of alumina oxide fibers provided sufficient sample for duplicate runs of each metal. The final metal loading for alumina and biomass-only samples ranged between 1-2% metal by weight and was calculated by the difference in mass before and after impregnation (correcting for the weight of acetate).

While the alumina substrate is not chemically reactive under our pyrolysis conditions (initial experiments showed alumina weight loss of around 0.2-0.3% when pyrolyzed at 600 °C for one hour; the manufacturer's tolerance guarantees no more than 0.5% at 900 °C), the alumina may impact pyrolysis products as the pyrolysis vapors flow over its fibers. This could lead to heterogeneous reactions on the surface of the alumina (e.g. one could imagine a scenario where some tarry pyrolysis products coalesce on the surface and then crack or (re)devolatilize, which could alter the composition of the bio-oil and non-condensable gases. As such, a control run of pure alumina fibers was included to account for any effects of the alumina.

2.2 Pyrolysis and bio-oil generation

Samples were pyrolyzed in a 5 cm diameter quartz tube furnace (MTI single heating zone GSL-1100X). During pyrolysis, the furnace was purged with 100 mL/min of nitrogen (≤0.1% atmospheric O_2) supplied by a nitrogen gas generator (Parker Balston Model N2-04). Before the start of each experiment, the furnace was purged with N_2 for 25 minutes to remove oxygen.

Samples were initially heated to 110 °C for 30 minutes to remove residual moisture, then heated to 600 °C for 60 minutes. The furnace temperature was ramped at 10 °C/minute. To separate and collect the bio-oil, the pyrolysis vapors exiting the system were routed through two cold traps (Chemglass Schwartz drying tubes). The tubes were immersed in a mixture of dry ice and glycol. Downstream of the cold traps, the non-condensable gases were analyzed in real time via a residual gas analyzer (RGA; Extorr XT300M with Pfeiffer HiCube 80 Eco Vacuum), sampled via a 40 μm ID silica capillary. The RGA was tuned to detect the mass to charge (*m/z*) ratios of four gases: hydrogen (*m/z* = 2), carbon dioxide (*m/z* = 44), methane (*m/z* = 15), ethane (*m/z* = 27). Note that the non-dominant *m/z* peaks for methane and ethane are utilized because of interference. Methane's dominant peak (*m/z* = 16) corresponds with minor peaks for carbon dioxide and oxygen, and ethane's dominant peak (*m/z* = 28) corresponds with the dominant peaks for nitrogen and carbon monoxide. We note that the use of N_2 for pyrolysis and an RGA does limit our discussion of the mechanisms responsible for catalytic activity given the inability to parse out CO and N_2. However, the goal of the work was to understand the overarching behavior of *in situ* versus *ex situ* TM catalysts. Depending on the degree of deoxygenation, further work could involve running experiments in argon gas and using FTIR to further probe the gas composition and behavior. The MS peaks were normalized to the quantity of input biomass. The remaining gas outflow was vented into a fume hood.

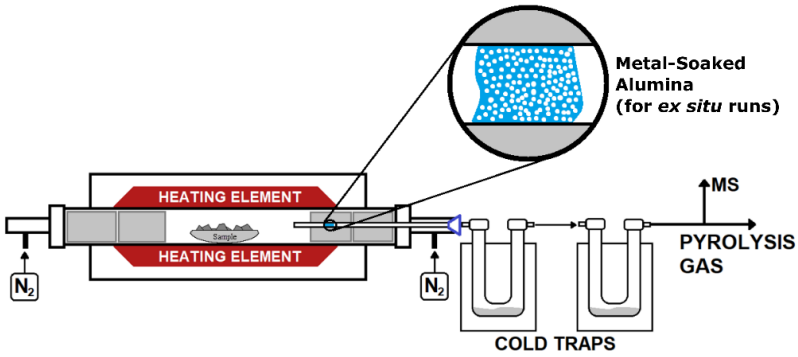

Fig. 1. Pyrolysis flow diagram and location of transition metals

For *in situ* catalysis runs, approximately 1.5 grams of TM-impregnated cherry pits or water-washed cherry pits, measured on a Shimadzu semi-microbalance (±0.1 mg) was placed in a porcelain combustion boat in the furnace. For *ex situ* catalysis, 1.5 grams of water-soaked cherry pit sample were placed in the porcelain combustion boat, with 0.15 grams of metal-soaked alumina fibers placed in a narrow vapor outlet tube downstream of the sample in the exhaust gas path. The alumina was set 5 cm back from the outlet to ensure minimal backflow after the pyrolysis gases contacted the alumina, and the alumina was stretched over a 3 cm section of the pipe to ensure the same packing density of the fibers across all runs. The alumina is still contained within the furnace, as seen in the diagram in Figure 1. The alumina experiences the same furnace temperatures as the pyrolyzing sample, as measured by a type-K thermocouple inserted into the alumina during a test (no-biomass run). The *ex situ* experiments have no direct contact between the biomass solid and catalyst. Only material volatilizing and leaving the biomass sample in the gaseous phase contacts the catalyst.

2.3 Bio-oil extraction and characterization

After pyrolysis, once the furnace cooled to below 100 °C, the purge gas was shut off and the cold traps were removed from the dry ice and glycol baths. The exterior of the cold traps was

198 immediately wiped clean of excess glycol and the traps weighed. The weight gain of the two
199 traps represents the bio-oil + water generated during the pyrolysis run. 10 mL of HPLC grade
200 (≥99%) dichloromethane (DCM) was used to rinse the cold traps and pull as much of the oil into
201 solution as possible. Parts of the aqueous phase and other non-DCM soluble oil remained
202 adhered to the cold traps, and the weight difference before and after the DCM rinse constituted
203 the 'non-recoverable' oil. Before analyzing the bio-oil samples with gas chromatography mass
204 spectroscopy (GC-MS), anhydrous magnesium sulfate (AMS; Fisher Scientific) was used to
205 remove water from the bio-oil. Approximately 0.2 grams of AMS (weighed on a Shimadzu semi-
206 microbalance to the 0.1 mg) was placed into a 1.5 mL microcentrifuge tube to which
207 approximately 1.0 mL of the collected bio-oil/DCM mixture was added. The tube was capped
208 and weighed again to determine the mass of bio-oil/DCM added. The centrifuge tube was shaken
209 for 5 minutes, then spun to separate the AMS/water and bio-oil. The now dried bio-oil/DCM
210 mixture was diluted further at a ratio of 0.6 mL DCM to 0.4 mL bio-oil mixture. The solid (now
211 hydrated) magnesium sulfate was allowed to dry in the fume hood overnight to remove any
212 surface volatiles, and the hydrated magnesium sulfate was weighed to determine the amount of
213 water present in the bio-oil.
214
215 *2.4 GC-MS analysis*
216 The diluted bio-oil was analyzed with a Shimadzu QP2020 gas chromatography mass
217 spectrometer with AOC-20i autosampler on a crossbond 30 m long 0.25 mm ID silica column.
218 Samples were injected with a 15:1 split ratio at 250 °C at an initial oven temperature of 40 °C,
219 purged with 1 mL/min of helium (Airgas UHP-300). The oven was held at 40 °C for 5 minutes,
220 then ramped at 5 °C/min to 150 °C where it held for an additional 5 minutes. The oven

temperature was increased at 1.75 °C/min to 250 °C with a final 10-minute hold. The mass spectrometer scanned between 15-400 *m/z* after a 6-minute solvent cut time. The resulting peaks were filtered (slopes ≥ 900, duration ≥ 2 seconds) and identified by matching spectra with the internal NIST libraries. [47–49]

The GC-MS was calibrated with 26 marker compounds in DCM (see supplemental information) on a 5-point calibration curve with concentrations ranging from 10 ppm to 1500 ppm . The total list of GC-MS identified compounds has over 200 entries, such that it is not possible to calibrate for every compound. Instead, peaks are matched to their most similar calibrated neighbor, based on Tanimoto similarity and molar mass. Similar compounds are separated and detected by GC-MS similarly, so while their response is not a perfect match, this method results in an accurate approximation and is similar to other approximation methods [47–49]. Identified compounds are split into their functional group and their relative mass fraction. The approach of splitting compounds into functional groups is more precise than attributing one functional group to each compound when compounds have multiple functional groups. The aggregated results for each functional group in each sample are computed by multiplying the concentration of each compound by the fraction of a functional group and summing for all compounds in the sample.

2.5 Biochar elemental analysis

Biochar samples were analyzed in triplicate on a CE-440 elemental analyzer from Exeter Analytical to determine carbon, hydrogen, and nitrogen content (oxygen by difference) via ASTM 5373-21. The calibration of the CE-440 analyzer used 1.8 mg acetanilide (≥ 99.99%, Lot# 0240-1121, Exeter Analytical) at 650 °C and 980 °C

3. Results and Discussion

Cherry pits were pyrolyzed using either *in situ* and *ex situ* TM catalysts whose loadings are described in Table 1 (average reported; replicate data available in SI).

3.1 Product yields

The effects of *in situ* and *ex situ* transition metal catalysts on product formation were investigated through product yields (Table 1). The overall liquid yield results are consistent with literature [50–52]. A statistically significant increase is observed for the bio-oil yield (unpaired two-tailed t-test, $p < 0.05$) between the control CP and *in situ* samples for Cu, Mn, and Zn, though the difference between the water contents for each of these samples is not statistically significantly difference. The raw CP and *in situ* CP+Ni are roughly equivalent in terms of organic bio-oil yield, and though in Figure 2 the Ni appears to have a lower water and higher total liquid yield, the differences are not statistically significant, nor are the differences in biochar or gas yield (including that of Ni, which does appear lower than all others). This suggests that the Cu, Mn and Zn are enhancing devolatilization of the biomass matrix though not necessarily reactions that would lead to fragmentation of volatiles to non-condensable gases. While the total liquid yields for the *in situ* and *ex situ* pure cherry pits are roughly equivalent, the *ex situ* sample has a considerably higher bio-oil yield than that of the *in situ* run the bio-oil yield (25.3 wt% versus 15.5 wt%, $p < 0.02$), such that the *in situ* run produces more water. As shown in Figure 2, given that the biochar yields are quite similar (meaning that both samples devolatilized roughly the same amount of volatile matter), this suggests that the inert alumina support may well impact gas phase reactions (e.g. limiting recombination of water). The alumina-supported Cu, Mn, and Ni runs shows similar water content to the CP+Alumina (and

Zn, while higher, is not statistically significantly different than the other samples). While the *ex situ* Cu pyrolysis yielded approximately the same amount of bio-oil as the CP+Alumina, the bio-oil yield for Mn, Ni and Zn was quite lower. As the char yields are roughly equivalent (as would be expected as the catalyst is downstream), the difference is made up with considerably higher gas yields. This suggests that the Mn, Ni and Zn are cracking the devolatilized molecules, increasing non-condensable gas formation.

Table 1. Pyrolysis product yields and ultimate analysis as a function of metal catalyst loading; average ± one standard deviation (*by difference)

	Pyrolysis Product Yields (wt%)				**Metal Loading (wt%)**
	Bio-oil	Water	Biochar	Gas*	
in situ experiments					
CP	15.5 ± 4.4	26.9 ± 7.1	24.9 ± 0.3	32.7 ± 11.8	-
CP+Cu	37.4 ± 11.6	13.2 ± 0.8	24.9 ± 0.1	24.6 ± 15.6	1.56 ± 0.05
CP+Mn	40.4 ± 15.4	12.0 ± 5.2	25.9 ± 0.3	21.7 ± 20.2	1.29 ± 0.03
CP+Ni	17.8 ± 8.5	18.4 ± 6.3	20.5 ± 3.7	43.3 ± 13.6	1.42 ± 0.07
CP+Zn	46.6 ± 1.8	15.8 ± 3.4	25.5 ± 0.3	12.1 ± 2.1	1.12 ± 0.01
ex situ experiments					
CP+Alumina	25.3 ± 0.6	14.8 ± 6.0	26.4 ± 0.4	33.6 ± 0.6	-
CP+Alumina Cu	28.5 ± 2.6	14.3 ± 0.6	26.2 ± 0.2	30.9 ± 4.1	1.77 ± 0.24
CP+Alumina Mn	12.3 ± 2.6	13.4 ± 3.1	26.2 ± 0.3	48.1 ± 5.7	1.16 ± 0.08
CP+Alumina Ni	15.8 ± 5.9	16.4 ± 6.3	26.3 ± 0.3	41.5 ± 12.2	1.70 ± 0.03
CP+Alumina Zn	10.0 ± 4.9	22.3 ± 10.1	25.8 ± 0.1	41.9 ± 15.9	2.07 ± 0.33

	Ultimate Analysis (wt% dry, ash-free basis)			
	Carbon	Hydrogen	Nitrogen	Oxygen*
Raw CP	51.6 ± 0.1	6.8 ± 0.0	3.8 ± 0.0	36.7 ± 0.1
in situ experiments				
CP	81.4 ± 0.1	1.9 ± 0.1	0.6 ± 0.0	16.2 ± 0.1
CP+Cu	79.3 ± 2.3	1.8 ± 0.1	0.6 ± 0.0	18.3 ± 2.2
CP+Mn	83.4 ± 2.2	1.8 ± 0.0	0.6 ± 0.0	14.2 ± 2.2
CP+Ni	72.8 ± 1.7	1.7 ± 0.0	0.6 ± 0.4	24.9 ± 1.4
CP+Zn	78.6 ± 2.8	1.8 ± 0.0	0.7 ± 0.0	18.9 ± 2.8
ex situ experiments				
CP+Alumina	76.3 ± 1.8	1.8 ± 0.1	0.6 ± 0.0	21.4 ± 1.9
CP+Alumina Cu	76.9 ± 6.7	1.8 ± 0.1	0.8 ± 0.7	19.9 ± 6.1
CP+Alumina Mn	78.1 ± 2.1	1.8 ± 0.1	0.6 ± 0.1	19.6 ± 2.2
CP+Alumina Ni	72.8 ± 2.3	1.8 ± 0.1	0.7 ± 0.0	24.8 ± 2.4
CP+Alumina Zn	77.9 ± 0.0	1.5 ± 0.0	2.1 ± 0.0	19.4 ± 0.0

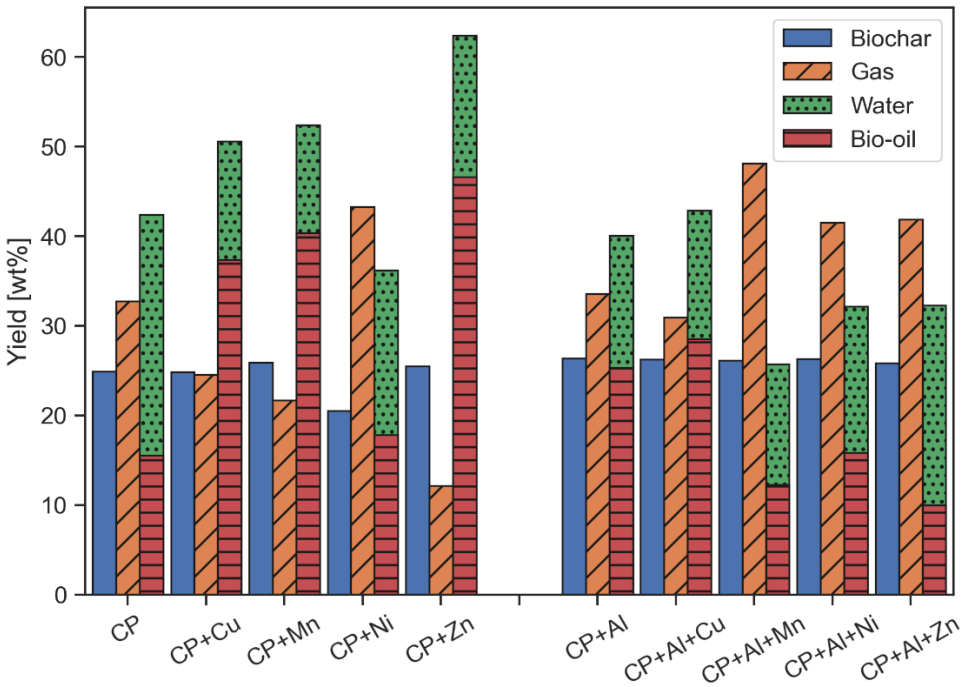

Figure 2. Pyrolysis experiment yields where liquid collected is separated into water and bio-oil phase in stacked bar; CP+metal data on left indicate *in situ* experiments; CP+Al+metal on right indicate *ex situ* experiments

3.2 Pyrolysis bio-oil

Figure 3 reports the mass fraction of each functional group in the bio-oils, computed by multiplying the concentration of each compound by the fraction of each functional group in the compound and summing over all compounds in the sample. There is considerable heterogeneity in the bio-oil samples themselves across the duplicate runs, in particular for the *in situ* nickel samples (individual sample analysis available in SI). However, the heterogeneity in terms of raw GC-MS chromatogram area data across duplicates is related to the mass of oil recovered, and not the representative quality. When we investigate the relative concentration profile of the duplicate samples, we see increasingly clearer trends emerge across TMs and catalyst placement. Figure 3 shows the average ratio of bio-oil components produced in each functional group to the aromatic carbon content computed by dividing the GC area for all compounds exhibiting a particular

functional group by that of the aromatic carbon's area for that sample and averaged across duplicates.

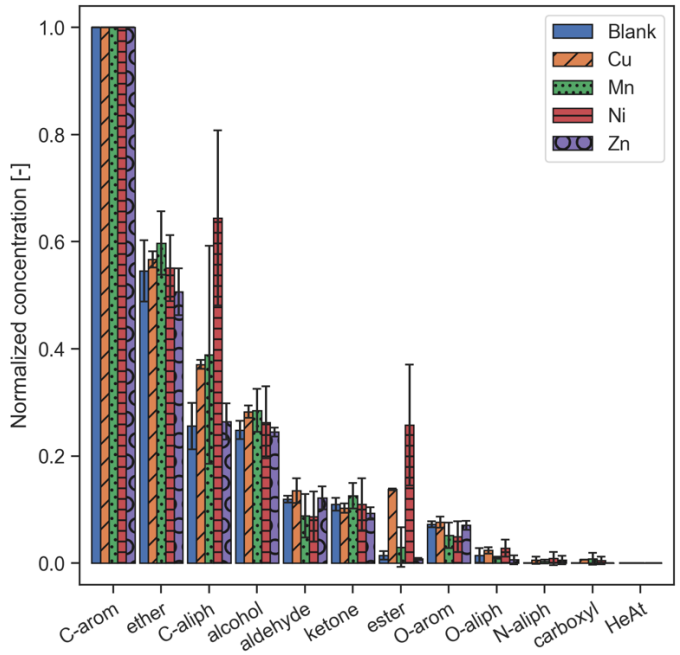

a. Bio-oil from *in situ* pyrolysis

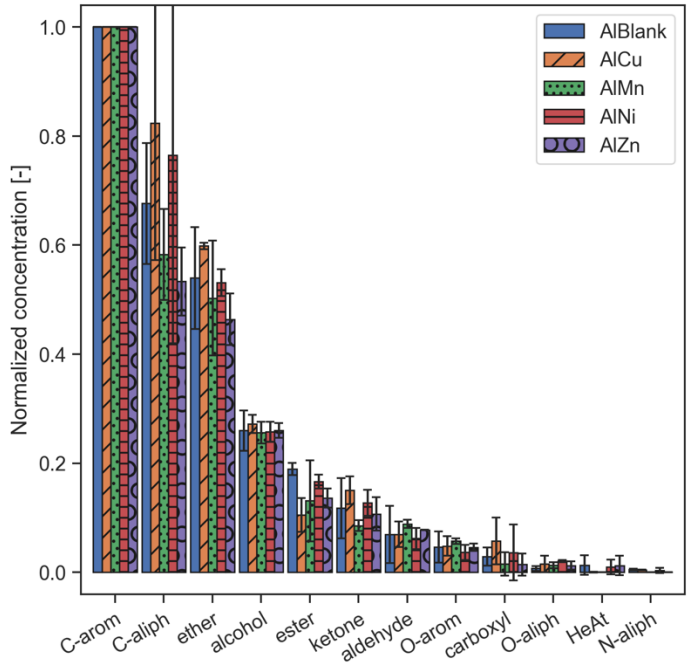

b. Bio-oil from *ex situ* pyrolysis

Figure 3. Bio-oil broken into functional groups normalized to aromatic carbon content (C-arom = aromatic carbons; C-aliph = aliphatic carbons; O-arom/O-aliph = aromatics/aliphatics containing oxygen heteroatoms; N-aliph = aliphatics containing nitrogen heteroatoms)

To generate an improved bio-oil, reducing oxygen-containing functional groups is desirable, with exceptions for fuel-necessary components such as alcohols [53,54]. Ethers and alcohols account for the majority of oxygen-containing functional groups, with carboxylic acid and esters representing an almost negligible quantity. If alcohol-containing compounds are targeted, it appears that manganese and zinc, when used as *in situ* catalysts, and manganese, nickel and zinc supported on alumina used as *ex situ* catalysts shifts towards higher alcohol quantities. When used *in situ,* zinc may promote the formation of aldehydes ($p < 0.05$), but the effect is minimal, and aldehydes represent a fairly small fraction of the overall bio-oil. The lack of significant compositional differences in the bio-oils resulting from the *in situ* metal experiments, Figure 3a, again point to the bio-oils role in enhancing devolatilization but of less potential to tune the bio-oil composition than the downstream catalysts.

Across the *ex situ* experiments, the bio-oil from Cu-based runs is not statistically significantly different from the alumina-only runs, though may perhaps shift some aromatic to aliphatics. Whereas there is scant effect on the ratios of aromatic carbons to other compounds and of overall bio-oil quality for the *in situ* runs, the *ex situ* experiments suggest a different story.
Mn may result in the opposite effect as overall there is a statistically significant increase in the aromatic carbon content of the Mn-based bio-oils versus the alumina blank ($p < 0.05$; see SI), though the ratios of C-aromatic to C-aliphatic are not statistically significantly different. Versus the alumina blank, Mn enhances the ether, alcohol ketone, aldehyde and oxygen-containing aromatic content of the bio-oil, with the ether and alcohol portion (relative to the aromatic carbon content) seeing the greatest change (Figure 3). The relative concentrations of ethers, alcohols and aldehydes increases for Ni and Zn bio-oils as well.

Oxygen concentration is calculated by multiplying each oxygen present in the oil by the concentration (ppm) of the corresponding compound. Oxygens across all compounds are summed to provide a total amount of oxygen present in the (dry) bio-oil. Figure 4 illustrates the van Krevelen diagram for the bio-oil. The van Krevelen diagram for bio-oil was generated by quantifying the compounds present, and using their total hydrogen, carbon, and oxygen counts to develop the molar O/C and H/C ratios. This analysis therefore represents the entire composition of the oil and is not limited to functional groups.

With the exception of the *ex situ* Zn sample, all of the alumina-supported metal bio-oils (represented by the open circle data points on Figure 4) have a statistically significantly ($p < 0.05$) reduced O/C ratio versus the *in situ* catalyzed runs (and CP), and most have improved H/C ratios. The *ex situ* Mn bio-oil has the highest H/C ratio of all the bio-oils examined, though the degree of deoxygenation among all of the *ex situ* runs is not statistically significant. Interestingly, we see a significant decrease in O/C and increase in H/C for even the alumina blank versus all of the *in situ* samples. This suggests that the alumina is preventing condensation of oxygenated tars in the bio-oil and/or cracking compounds to produce more non-condensable gases. We do note, however, that the changes in these ratios are quite small (as evidenced by the scales in Figure 4) though in line with other pyrolysis bio-oils.

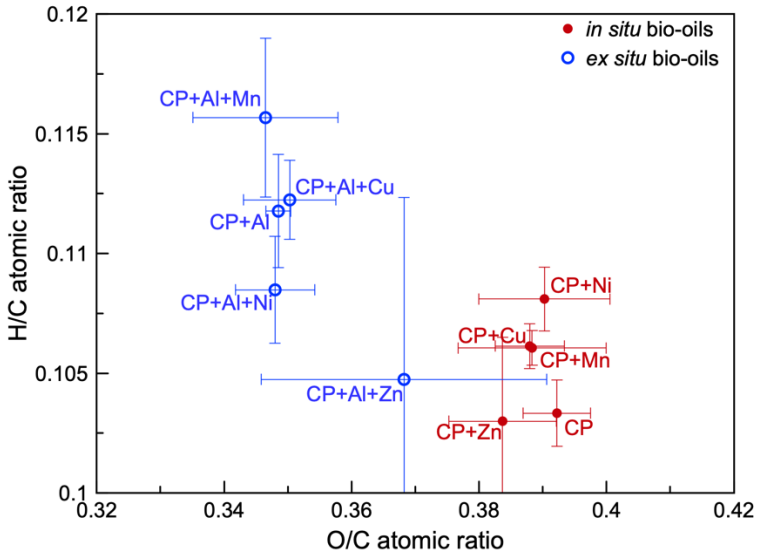

Figure 4. van Krevelen diagram of bio-oils made via *in situ* versus *ex situ* pyrolysis of cherry pits (error bars equal to one standard deviation)

3.3 Biochar composition

With decreased O/C and increased H/C ratios in the bio-oil for alumina-metal catalysts, the changes in the solid biochar phase could serve as indicators of solid vs. vapor phase interactions. Whereas the alumina-metal catalysts are situated downstream and are poised to catalyze the vapor phase, the direct mixing of biomass and metal (in the *in situ* cases) has the potential to alter the biomass to biochar conversion and composition. Figure 5 highlights the change in composition of the biochar on a van Krevelen diagram. Unlike in the oil phase, the char is not distributed into 'alumina' and 'no-alumina' regions, but instead we see a range of compositions without a clear trend based on catalyst or its location.

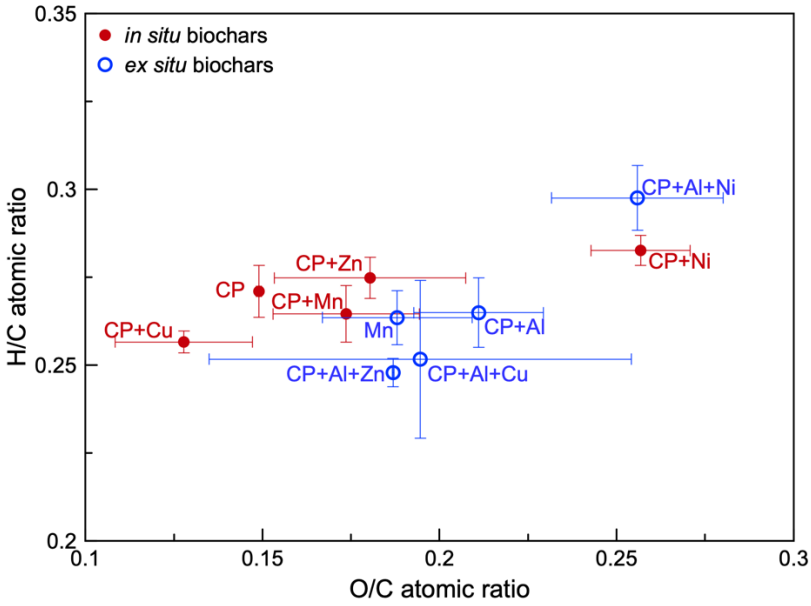

Figure 5. van Krevelen diagram of biochars made via *in situ* versus *ex situ* pyrolysis of cherry pits (error bars equal to one standard deviation)

The lack of statistically significant differences between the *ex situ* run biochars (with the exception of the Ni) is expected considering that these cases do not allow for the alumina impregnated metal to contact the biochar. The samples with *in situ* metals can alter the composition of the biochar, however all the downstream *ex situ* metals would only act on compounds that have entered the gas phase (and should have no opportunity to recondense on the biochar). The lack of significant differences among the *in situ* samples indicates that the *in situ* metals may catalyze the overall devolatilization, but that their ability to chemically change the biochar and bio-oil/gas is limited when used *in situ*. The muted effects of the *in situ* metals is potentially due to coking [55], deactivation [56], or limits on heat/mass transfer [57] where the metals become unable to interact with the vapor phase.

Throughout our analyses – despite multiple replicates – the use of Ni in both *in situ* and *ex situ* runs appears to be a bit of an outlier. The bio-oils are rather heterogeneous, negating any

statistically significant observations. In the solid products, both catalyst placements lead to biochars with slightly higher oxygen to carbon ratios than any other sample. While for *in situ* positioning this could mean that the catalyst spurs oxidation of the biochar, this is more difficult to interpret for the *ex situ* samples. One plausible explanation is that the Ni-supported alumina catalyzes reactions that release fairly significant amounts of oxidizing gases (CO, O_2), of which some back mix near the biochar and oxidize the surface. This could be decarboxylation of the O-aromatic compounds in the pyrolysis bio-oil, which are reduced for both Ni samples. Given the high gas sweep rate this seems unlikely, however (to date) it is the most plausible explanation we have found, and we look forward to engaging with the field further in determining the root causes for these observations.

3.4 Non-condensable gas formation

Carbon dioxide is a major gaseous product of all the pyrolysis reactions (Figure 6) that provides a direct measure of oxygen leaving the system. The *in situ* cases result in mixed outcomes, with nickel generating an increase in CO_2 production by 44%, likely due to the added activity near the reaction hold temperature of 600 °C (between 80-100 minutes). Manganese and zinc see similar increases in CO_2 production (20% and 43% respectively), however copper experiences a slight decrease of 7%. The *ex situ* experiments, where the evolved gas is passed over the alumina-soaked catalyst downstream, yield an altogether larger quantity of CO_2 compared to the *in situ* cases (note the change in axis scaling by nearly an order of magnitude).

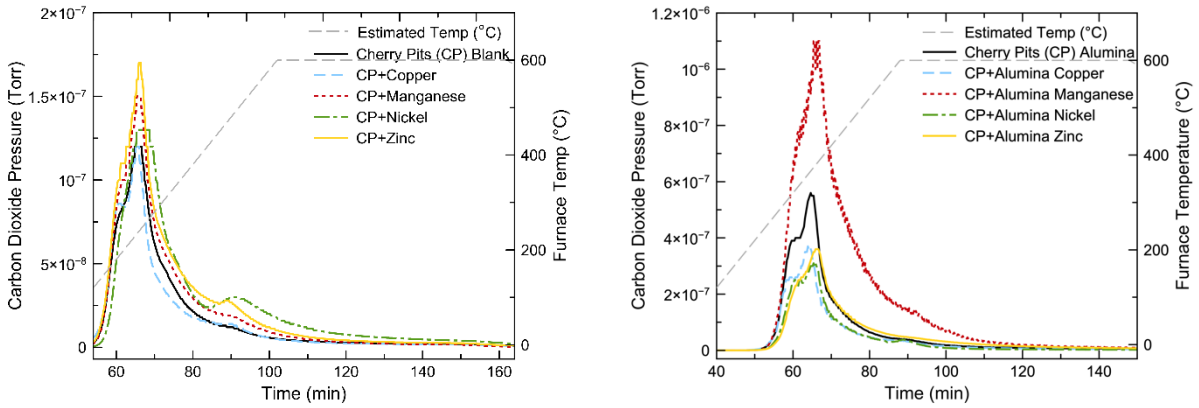

a. CO_2 for *in situ* pyrolysis experiments b. CO_2 for *ex situ* pyrolysis experiments

Figure 6. CO_2 in evolved pyrolysis gas for *in situ* and *ex situ* transition metal catalysis; pressure normalized to sample mass.

The inclusion of the alumina oxide – without the addition of transition metals – enhances CO_2 production itself. This is likely due to the improved heat transfer effects on the gas passing through a heated porous material, which can be demonstrated by the disparity in their heat capacity. While an exact figure for the heat capacity of cherry pit biochar is not known, graphite can be used as a conservative stand-in, since the biochar begins to graphitize as the temperature in the furnace rises to pyrolysis conditions. This gives a conservative estimate for C_p as high as 20 J/molK (at 1000K) [58], which is still far less than the downstream alumina counterpart at 120 J/molK (at 1000K) [59]. Alumina's higher heat capacity translates to smaller variations in temperature during pyrolysis as the relatively cool nitrogen gas has a smaller cooling effect on the alumina, and the alumina retains heat (and therefore energy) for a longer duration after heating. While the particles have been finely ground (1-2mm), improving the heat transfer across any given particle assists in its devolatilization by providing the energy needed to move to a lower-energy oxidized state [60]. The alumina possibly provides nucleation sites for the vapor phase to interact at high temperatures [61]. However, the effects of the inclusion of manganese

411 are magnified greatly by the *ex situ* alumina. Instead of the 20% increase in CO_2 production as
412 seen for Mn versus raw CP *in situ*, the *ex situ* manganese impregnated alumina increases CO_2
413 production by 148%, or nearly 2.5 times. These trends continue for *ex situ* hydrogen, methane,
414 and ethane, with manganese impregnated alumina generating gases far above the baseline.
415 Various forms of manganese have been used in a wide array of catalytic reactions due to the
416 numerous oxidation states, ranging from the targeting of C-H hydroxylation to assist with the
417 'magic methyl effect' [62], to promoting oxidation of CO waste streams [63]. The concentrations
418 of available oxygen and operating temperature affect the form manganese oxides commonly take
419 as either MnO_2, Mn_2O_3, or Mn_3O_4 [64,65] though more states exist. This variable oxidation state
420 allows manganese to act as either an oxidizing or reducing agent. Despite the inert nature of
421 alumina oxide at temperatures below 1000 °C, some mass loss is expected (manufacturer reports
422 $\leq$ 5%). Excess oxygen present from the Al_2O_3 may interact with the manganese to form more
423 productive species than its *in situ* counterpart. Higher oxygen contents and lower temperatures
424 have shown to favor the formation of MnO_2 [63] which may account for the difference in
425 activity.
426
427 The increased generation of carbon dioxide for the manganese and alumina catalyst is a strong
428 indicator that oxygen is being removed from the bio-oil via decarboxylation, as confirmed by the
429 drop and increase in the O/C and H/C ratio for the *in situ* versus the *ex situ* experiments, in
430 Figure 4 respectively. By removing the oxygen from the liquid phase, the bio-oil can be
431 fragmented into smaller oil compounds with reduced acidity and instability [66].
432

The *ex situ* manganese samples outperform other *ex situ* metals (and *in situ* metals) in the production of hydrogen, methane, and ethane (plots available in supplemental information). Metals used *in situ* generate hydrogen to varying degrees, with copper producing nearly the same amount as the baseline, and manganese, zinc, and nickel producing 50% (± 6%), 84% (± 17%), 192% (± 67%) more hydrogen gas respectively. This increase in hydrogen gas production is advantageous. Hydrogen can be separated and used as its own renewable fuel, either through direct combustion of H_2 gas or fuel cell use [67,68]. Furthermore, this release of hydrogen gas can be indicative of increased fragmentation of the vapor phase, potentially leading to smaller, more desirable, bio-oil compounds (hydrocracking) [69]. Previous studies show that thermochemical reactions of lignin without a hydrogen donor tend to repolymerize intermediates to form more solids via hydrogenolysis of β-O-4 and α-O-4 bonds [70,71], adversely affecting bio-oil yield and quality. Additionally, hydrogen can be used in catalytic cracking reactions such as hydrogenation to increase the saturation of compounds, which leads to fuels producing less CO_2 when burned [69].

3.5. Summary and Future Work

The present work sheds insight into the relative levels of deoxygenation achievable with single TM catalysts. TM are often complexed with sulfides (forming transition metal sulfides) and used for hydrogenation, Fischer-Tropsch and heteroatom removal in refineries around the world. The role of the S is (likely) to activate molecular hydrogen to form S-H groups and catalyze hydrodeoxygenation. As reported by Ruddy *et al*., the relative reactivities of oxygenated compounds on transition metal sulfides is roughly: aliphatic alcohols > ketones > alkyl ethers > carboxylic acids ≈ m-/p-phenols ≈ naphthol > phenol > o-ethylphenol > dibenzofuran, with

456 furans being the least reactive of the pyrolysis bio-oil oxygen species. Given the lack of a sulfur
457 site to enable such coordination and dearth of hydrogen in the cherry pit feedstock used here, it is
458 interesting to see how the relative concentrations of alcohols versus aromatic carbons increases,
459 as do ketones and ethers, supporting the hypothesized role of the S in the TM sulfides. However,
460 given the increase in the ratio of water to bio-oil produced for the *ex situ* experiments, it is
461 reasonable to assert that these catalysts are participating in some degree of hydrodeoxygenation.
462
463 As the goal of this work was to explore fundamental science surrounding the impact of these TM
464 catalysts (1) without scaffolds or bifunctionality and (2) when used *in situ* versus *ex situ*, the
465 present work explores these TMs only as single-use catalysts, which is not industrially feasible
466 or sustainable. Future work – as is ongoing in our laboratory, with our industrial collaborators,
467 and beyond our lab – should explore the reclamation and reusability of TMs when used *in situ*,
468 and coking propensity and decoking required when used for downstream upgrading of pyrolysis
469 vapors. Finally, as most industrial processes for bio-oil are adopting fast (or even flash)
470 pyrolysis, the present work is useful in understanding how *in situ* versus *ex situ* schemes can
471 alter the product balance and degree of deoxygenation during versus after pyrolysis, but further
472 work should investigate how such processes scale in terms of pyrolysis heating rates.
473

474 **4. Conclusions**

475 This study examined the effect of using transition metals as *in situ* and *ex situ* catalysts as
476 alternatives to precious metals for the upgrading of pyrolysis bio-oils. Specifically, *ex situ* metals
477 supported on alumina, acting on the pyrolysis vapor phase, lowered the O/C ratio in the bio-oil
478 when compared to *in situ* metals and increased the H/C ratio for some metals (in particular Mn),

without drastically altering the composition of the biochar. Manganese-impregnated alumina demonstrated an ability to generate high quantities of pyrolysis gas, specifically H_2, CO_2, CH_4, and C_2H_6 when placed in the *ex situ* downstream position. By moving the catalyst downstream, the devolatilized compounds fragment into smaller, non-condensable gases, and increase the production of water, indicating a higher degree of hydrodeoxygenation. instead of heterogeneous surface-gas interactions on the biochar taking place at the solid-vapor interphase. Large, tarry (viscous, unstable, and oxygenated) compounds that pyrolyze into the vapor phase (and ultimately recondense in the bio-oil) can be addressed using *ex situ* downstream catalysts at relatively low temperatures (e.g. the same as pyrolysis). Conversely, *in situ* catalysts result in greater liquid production with lower water fractions than *ex situ* catalysts. In particular, Mn, Ni and Zn boost the relative concentrations of ethers and alcohols in the resulting bio-oils as compared to uncatalyzed or Cu-catalyzed biomass. However, because of coking and deactivation, the use of such *in situ* catalysts in fixed bed pyrolysis may be limited.

CRediT authorship contribution statement

Andrew H. Hubble: Conceptualization, Methodology, Investigation, Data analysis, Writing – original draft. **Bridget A. Childs:** Investigation, Initial data analysis. **Matteo Pecchi:** Data analysis, Data Visualization, Writing – review and editing. **Hanifrahmawan Sudibyo:** Investigation, Writing – review and editing. **Jefferson W. Tester:** Resources, Writing – review and editing. **Jillian L. Goldfarb:** Conceptualization, Resources, Funding acquisition, Supervision, Writing – revised draft.

Declaration of Competing Interest

The authors declare that they have no known competing financial interests or personal relationships that could have influenced the work reported in this paper.

Acknowledgements

This work was supported by the National Science Foundation under CBET grant number 1933071. This work was partially supported by a Hatch Grant under accession number 1021398 from the USDA National Institute of Food and Agriculture.

References

[1] M.R. Allen, O.P. Dube, W. Solecki, F. Aragón-Durand, W. Cramer, S. Humphreys, M. Kainuma, J. Kala, N. Mahowald, Y. Mulugetta, R. Perez, M.Wairiu, K. Zickfeld, 2018: Framing and Context. In: Global Warming of 1.5°C. An IPCC Special Report on the impacts of global warming of 1.5°C above pre-industrial levels and related global greenhouse gas emission pathways, in the context of strengthening the global response, Australia, 2018.

[2] The White House Briefing Room, Biden Administration Advances the Future of Sustainable Fuels in American Aviation, (2021). https://www.whitehouse.gov/briefing-room/statements-releases/2021/09/09/fact-sheet-biden-administration-advances-the-future-of-sustainable-fuels-in-american-aviation/ (accessed January 24, 2022).

[3] L. Cai, F. vom Lehn, H. Pitsch, Higher Alcohol and Ether Biofuels for Compression-Ignition Engine Application: A Review with Emphasis on Combustion Kinetics, Energy & Fuels. 35 (2021) 1890–1917. https://doi.org/10.1021/ACS.ENERGYFUELS.0C03590.

[4] T.K. Phung, A.A. Casazza, P. Perego, P. Capranica, G. Busca, Catalytic pyrolysis of vegetable oils to biofuels: Catalyst functionalities and the role of ketonization on the oxygenate paths, Fuel Processing Technology. 140 (2015) 119–124. https://doi.org/10.1016/J.FUPROC.2015.08.042.

[5] X. Hu, R. Gunawan, D. Mourant, M.D.M. Hasan, L. Wu, Y. Song, C. Lievens, C.Z. Li, Upgrading of bio-oil via acid-catalyzed reactions in alcohols — A mini review, Fuel Processing Technology. 155 (2017) 2–19. https://doi.org/10.1016/J.FUPROC.2016.08.020.

[6] W. Cai, R. Liu, Y. He, M. Chai, J. Cai, Bio-oil production from fast pyrolysis of rice husk in a commercial-scale plant with a downdraft circulating fluidized bed reactor, Fuel Processing Technology. 171 (2018) 308–317. https://doi.org/10.1016/J.FUPROC.2017.12.001.

[7] M. Garca-Pèrez, A. Chaala, C. Roy, Vacuum pyrolysis of sugarcane bagasse, J Anal Appl Pyrolysis. 65 (2002) 111–136. https://doi.org/10.1016/S0165-2370(01)00184-X.

[8] P. Li, X. Shi, X. Wang, J. Song, S. Fang, J. Bai, G. Zhang, C. Chang, S. Pang, Bio-oil from biomass fast pyrolysis: Yields, related properties and energy consumption analysis of the pyrolysis system, J Clean Prod. 328 (2021) 129613. https://doi.org/10.1016/J.JCLEPRO.2021.129613.

[9] G.V. Brigagão, O. de Queiroz Fernandes Araújo, J.L. de Medeiros, H. Mikulcic, N. Duic, A techno-economic analysis of thermochemical pathways for corncob-to-energy: Fast pyrolysis to bio-oil, gasification to methanol and combustion to electricity, Fuel Processing Technology. 193 (2019) 102–113. https://doi.org/10.1016/J.FUPROC.2019.05.011.

[10] H. Wang, R. Gunawan, Z. Wang, L. Zhang, Y. Liu, S. Wang, M.D.M. Hasan, C.Z. Li, High-pressure reactive distillation of bio-oil for reduced polymerisation, Fuel Processing Technology. 211 (2021) 106590. https://doi.org/10.1016/J.FUPROC.2020.106590.

[11] B. Zheng, Y. Shen, P. Sun, R. Liu, J. Meng, R. Chang, T. Gao, Y. Liu, Effects of particle sizes on performances of the multi-zone steam generator using waste heat in a bio-oil steam reforming hydrogen production system, Int J Hydrogen Energy. 46 (2021) 18064–18072. https://doi.org/10.1016/J.IJHYDENE.2020.10.269.

549 [12] T. Cordero-Lanzac, J. Rodríguez-Mirasol, T. Cordero, J. Bilbao, Advances and Challenges in the
550 Valorization of Bio-Oil: Hydrodeoxygenation Using Carbon-Supported Catalysts, Energy & Fuels.
551 35 (2021) 17008–17031. https://doi.org/10.1021/ACS.ENERGYFUELS.1C01700.

552 [13] N. Chaihad, A. Anniwaer, A. Choirun Az Zahra, Y. Kasai, P. Reubroycharoen, K. Kusakabe, A.
553 Abudula, G. Guan, In-situ catalytic upgrading of bio-oil from rapid pyrolysis of biomass over
554 hollow HZSM-5 with mesoporous shell, Bioresour Technol. 341 (2021) 125874.
555 https://doi.org/10.1016/J.BIORTECH.2021.125874.

556 [14] N. Chaihad, A. Anniwaer, S. Karnjanakom, Y. Kasai, S. Kongparakul, C. Samart, P. Reubroycharoen,
557 A. Abudula, G. Guan, In-situ catalytic upgrading of bio-oil derived from fast pyrolysis of sunflower
558 stalk to aromatic hydrocarbons over bifunctional Cu-loaded HZSM-5, J Anal Appl Pyrolysis. 155
559 (2021) 105079. https://doi.org/10.1016/J.JAAP.2021.105079.

560 [15] L. Mo, H. Dai, L. Feng, B. Liu, X. Li, Y. Chen, S. Khan, In-situ catalytic pyrolysis upgradation of
561 microalgae into hydrocarbon rich bio-oil: Effects of nitrogen and carbon dioxide environment,
562 Bioresour Technol. 314 (2020) 123758. https://doi.org/10.1016/J.BIORTECH.2020.123758.

563 [16] C.T. Zhang, L. Zhang, Q. Li, Y. Wang, Q. Liu, T. Wei, D. Dong, S. Salavati, M. Gholizadeh, X. Hu,
564 Catalytic pyrolysis of poplar wood over transition metal oxides: Correlation of catalytic behaviors
565 with physiochemical properties of the oxides, Biomass Bioenergy. 124 (2019) 125–141.
566 https://doi.org/10.1016/J.BIOMBIOE.2019.03.017.

567 [17] Y. Han, M. Gholizadeh, C.C. Tran, S. Kaliaguine, C.Z. Li, M. Olarte, M. Garcia-Perez,
568 Hydrotreatment of pyrolysis bio-oil: A review, Fuel Processing Technology. 195 (2019) 106140.
569 https://doi.org/10.1016/J.FUPROC.2019.106140.

570 [18] W. Choi, H. Jo, J.W. Choi, D.J. Suh, H. Lee, C. Kim, K.H. Kim, K.Y. Lee, J.M. Ha, Stabilization of acid-
571 rich bio-oil by catalytic mild hydrotreating, Environmental Pollution. 272 (2021) 116180.
572 https://doi.org/10.1016/J.ENVPOL.2020.116180.

573 [19] T. Cordero-Lanzac, R. Palos, I. Hita, J.M. Arandes, J. Rodríguez-Mirasol, T. Cordero, J. Bilbao, P.
574 Castaño, Revealing the pathways of catalyst deactivation by coke during the hydrodeoxygenation
575 of raw bio-oil, Appl Catal B. 239 (2018) 513–524. https://doi.org/10.1016/J.APCATB.2018.07.073.

576 [20] A.S. Amarasekara, C.D. Gutierrez Reyes, Pd/C catalyzed room-temperature, atmospheric pressure
577 hydrogenation of furanic bio-oils from acidic ionic liquid catalyzed liquefaction of biomass in
578 acetone, Fuel Processing Technology. 200 (2020) 106320.
579 https://doi.org/10.1016/J.FUPROC.2019.106320.

580 [21] Y. Zheng, J. Wang, D. Li, C. Liu, Y. Lu, X. Lin, Z. Zheng, Highly efficient catalytic pyrolysis of biomass
581 vapors upgraded into jet fuel range hydrocarbon-rich bio-oil over a bimetallic Pt–Ni/γ-Al2O3
582 catalyst, Int J Hydrogen Energy. 46 (2021) 27922–27940.
583 https://doi.org/10.1016/J.IJHYDENE.2021.06.082.

584 [22] A.C. Dyer, M.A. Nahil, P.T. Williams, Biomass:polystyrene co-pyrolysis coupled with metal-
585 modified zeolite catalysis for liquid fuel and chemical production, J Mater Cycles Waste Manag.
586 24 (2022) 477–490. https://doi.org/10.1007/S10163-021-01334-0/FIGURES/11.

[23] Z. Li, E. Jiang, X. Xu, Y. Sun, R. Tu, Hydrodeoxygenation of phenols, acids, and ketones as model bio-oil for hydrocarbon fuel over Ni-based catalysts modified by Al, La and Ga, Renew Energy. 146 (2020) 1991–2007. https://doi.org/10.1016/J.RENENE.2019.08.012.

[24] Y. Feng, S. Long, X. Tang, Y. Sun, R. Luque, X. Zeng, L. Lin, Earth-abundant 3d-transition-metal catalysts for lignocellulosic biomass conversion, Chem Soc Rev. 50 (2021) 6042–6093. https://doi.org/10.1039/D0CS01601B.

[25] F. Chen, S. Yang, J. Hu, Q. Xiong, In Situ Catalytic Pyrolysis of Municipal Sewage Sludge under Calcined Copper Slag: Thermokinetic Analysis and Real-Time Monitoring of Evolved Gases, ACS Sustain Chem Eng. 10 (2022) 14381–14390. https://doi.org/10.1021/acssuschemeng.2c05218.

[26] M. Karod, A.H. Hubble, A.R. Maag, Z.A. Pollard, J.L. Goldfarb, Clay-catalyzed in situ pyrolysis of cherry pits for upgraded biofuels and heterogeneous adsorbents as recoverable by-products, Biomass Convers Biorefin. (2022). https://doi.org/10.1007/s13399-022-02921-3.

[27] K. Praserttaweeporn, T. Vitidsant, W. Charusiri, Ni-modified dolomite for the catalytic deoxygenation of pyrolyzed softwood and non-wood to produce bio-oil, Results in Engineering. 14 (2022) 100461. https://doi.org/10.1016/j.rineng.2022.100461.

[28] E. Balaghi Inaloo, M. Saidi, A. Taheri Najafabadi, Valuable Biofuel Production via Pyrolysis Process of Olive Pomace over Alkali and Transition Metal Oxides Catalysts Supported on Activated Biochar, ChemistrySelect. 7 (2022). https://doi.org/10.1002/slct.202200789.

[29] H. Yang, Z. Chen, W. Chen, Y. Chen, X. Wang, H. Chen, Role of porous structure and active O-containing groups of activated biochar catalyst during biomass catalytic pyrolysis, Energy. 210 (2020) 118646. https://doi.org/10.1016/j.energy.2020.118646.

[30] Y. Su, K. Fu, Y. Zheng, N. Ji, C. Song, D. Ma, X. Lu, R. Han, Q. Liu, Catalytic oxidation of dichloromethane over Pt-Co/HZSM-5 catalyst: Synergistic effect of single-atom Pt, Co3O4, and HZSM-5, Appl Catal B. 288 (2021) 119980. https://doi.org/10.1016/J.APCATB.2021.119980.

[31] Z. He, G. Yang, H. Wang, F. Dai, F. Peng, H. Yu, Co-N-C-Supported Platinum Catalyst: Synergistic Effect on the Aerobic Oxidation of Glycerol, ACS Sustain Chem Eng. 8 (2020) 19062–19071. https://doi.org/10.1021/ACSSUSCHEMENG.0C07332/SUPPL_FILE/SC0C07332_SI_001.PDF.

[32] B. Cifuentes, M. Hernández, S. Monsalve, M. Cobo, Hydrogen production by steam reforming of ethanol on a RhPt/CeO2/SiO2 catalyst: Synergistic effect of the Si:Ce ratio on the catalyst performance, Appl Catal A Gen. 523 (2016) 283–293. https://doi.org/10.1016/J.APCATA.2016.06.014.

[33] J. Resasco, F. Yang, T. Mou, B. Wang, P. Christopher, D.E. Resasco, Relationship between Atomic Scale Structure and Reactivity of Pt Catalysts: Hydrodeoxygenation of m-Cresol over Isolated Pt Cations and Clusters, ACS Catal. 10 (2020) 595–603. https://doi.org/10.1021/ACSCATAL.9B04330/SUPPL_FILE/CS9B04330_SI_001.PDF.

[34] I. Bodachivskyi, U. Kuzhiumparambil, D.B.G. Williams, Metal triflates are tunable acidic catalysts for high yielding conversion of cellulosic biomass into ethyl levulinate, Fuel Processing Technology. 195 (2019) 106159. https://doi.org/10.1016/J.FUPROC.2019.106159.

[35] D. Zhong, K. Zeng, J. Li, Y. Qiu, G. Flamant, A. Nzihou, V.S. Vladimirovich, H. Yang, H. Chen, Characteristics and evolution of heavy components in bio-oil from the pyrolysis of cellulose, hemicellulose and lignin, Renewable and Sustainable Energy Reviews. 157 (2022) 111989. https://doi.org/10.1016/J.RSER.2021.111989.

[36] Z. Xiong, Y. Xiong, Q. Li, H. Han, W. Deng, J. Xu, L. Jiang, S. Su, S. Hu, Y. Wang, J. Xiang, Effects of vapor-/solid-phase interactions among cellulose, hemicellulose and lignin on the formation of heavy components in bio-oil during pyrolysis, Fuel Processing Technology. 225 (2022) 107042. https://doi.org/10.1016/J.FUPROC.2021.107042.

[37] H. Weldekidan, V. Strezov, T. Kan, R. Kumar, J. He, G. Town, Solar assisted catalytic pyrolysis of chicken-litter waste with in-situ and ex-situ loading of CaO and char, Fuel. 246 (2019) 408–416. https://doi.org/10.1016/j.fuel.2019.02.135.

[38] K. Wang, P.A. Johnston, R.C. Brown, Comparison of in-situ and ex-situ catalytic pyrolysis in a micro-reactor system, Bioresour Technol. 173 (2014) 124–131. https://doi.org/10.1016/j.biortech.2014.09.097.

[39] K. Iisa, D.J. Robichaud, M.J. Watson, J. ten Dam, A. Dutta, C. Mukarakate, S. Kim, M.R. Nimlos, R.M. Baldwin, Improving biomass pyrolysis economics by integrating vapor and liquid phase upgrading, Green Chemistry. 20 (2018) 567–582. https://doi.org/10.1039/C7GC02947K.

[40] V. Frišták, D. Bošanská, M. Pipíška, L. Ďuriška, S.M. Bell, G. Soja, Physicochemical Characterization of Cherry Pits-Derived Biochar, Materials 2022, Vol. 15, Page 408. 15 (2022) 408. https://doi.org/10.3390/MA15020408.

[41] P. Yangali, A.M. Celaya, J.L. Goldfarb, Co-pyrolysis reaction rates and activation energies of West Virginia coal and cherry pit blends, J Anal Appl Pyrolysis. 108 (2014) 203–211. https://doi.org/10.1016/J.JAAP.2014.04.015.

[42] Z.A. Pollard, J.L. Goldfarb, Valorization of cherry pits: Great Lakes agro-industrial waste to mediate Great Lakes water quality, Environmental Pollution. 270 (2021) 116073. https://doi.org/10.1016/J.ENVPOL.2020.116073.

[43] G.M.A. Foreign Agricultural Service, Fresh Peaches and Cherries: World Markets and Trade, 2021. https://public.govdelivery.com/accounts/USDAFAS/subscriber/new (accessed March 6, 2022).

[44] United States Department of Agriculture: National Statistics for Cherries, National Agricultural Statistics Service, (2020). https://www.nass.usda.gov/Statistics_by_Subject/result.php?4DA594EC-B4CC-333F-9B93-929A52E35D50&sector=CROPS&group=FRUIT %26 TREE NUTS&comm=CHERRIES (accessed January 25, 2022).

[45] S. Haukka, E.L. Lakomaa, T. Suntola, Adsorption controlled preparation of heterogeneous catalysts, Stud Surf Sci Catal. 120 A (1999) 715–750. https://doi.org/10.1016/S0167-2991(99)80570-9.

[46] J.R.A. Sietsma, A. Jos van Dillen, P.E. de Jongh, K.P. de Jong, Application of ordered mesoporous materials as model supports to study catalyst preparation by impregnation and drying, Stud Surf Sci Catal. 162 (2006) 95–102. https://doi.org/10.1016/S0167-2991(06)80895-5.

[47] R. Olcese, V. Carré,Carré, F. Frédé, F. Aubriet, A. Dufour, Selectivity of Bio-oils Catalytic Hydrotreatment Assessed by Petroleomic and GC*GC/MS-FID Analysis, (2013). https://doi.org/10.1021/ef302145g.

[48] P.R. Patwardhan, R.C. Brown, B.H. Shanks, Understanding the Fast Pyrolysis of Lignin, ChemSusChem. 4 (2011) 1629–1636. https://doi.org/10.1002/CSSC.201100133.

[49] J.W. Ahn, S.K. Pandey, K.H. Kim, Comparison of GC-MS Calibration Properties of Volatile Organic Compounds and Relative Quantification Without Calibration Standards, J Chromatogr Sci. 49 (2011) 19–28. https://doi.org/10.1093/CHRSCI/49.1.19.

[50] S. Zhang, H. Zhang, X. Liu, S. Zhu, L. Hu, Q. Zhang, Upgrading of bio-oil from catalytic pyrolysis of pretreated rice husk over Fe-modified ZSM-5 zeolite catalyst, Fuel Processing Technology. 175 (2018) 17–25. https://doi.org/10.1016/J.FUPROC.2018.03.002.

[51] Y. Li, S. Hao, J. Shu, S. Zhang, J. Wang, C. Wang, N. Hou, Y. Li, Unraveling the role of reaction environment and catalysts for pyrolysis of technical lignin into different functional bio-oil yield, Journal of the Energy Institute. 100 (2022) 47–54. https://doi.org/10.1016/J.JOEI.2021.09.010.

[52] J. Fermoso, H. Hernando, S. Jiménez-Sánchez, A.A. Lappas, E. Heracleous, P. Pizarro, J.M. Coronado, D.P. Serrano, Bio-oil production by lignocellulose fast-pyrolysis: Isolating and comparing the effects of indigenous versus external catalysts, Fuel Processing Technology. 167 (2017) 563–574. https://doi.org/10.1016/J.FUPROC.2017.08.009.

[53] Y. Han, M. Gholizadeh, C.C. Tran, S. Kaliaguine, C.Z. Li, M. Olarte, M. Garcia-Perez, Hydrotreatment of pyrolysis bio-oil: A review, Fuel Processing Technology. 195 (2019) 106140. https://doi.org/10.1016/J.FUPROC.2019.106140.

[54] M.D.G. de Luna, L.A.D. Cruz, W.H. Chen, B.J. Lin, T.H. Hsieh, Improving the stability of diesel emulsions with high pyrolysis bio-oil content by alcohol co-surfactants and high shear mixing strategies, Energy. 141 (2017) 1416–1428. https://doi.org/10.1016/J.ENERGY.2017.11.055.

[55] L. Jia, C. Cao, Z. Cheng, J. Wang, J. Huang, J. Yang, Y. Pan, M. Xu, Y. Wang, Ex Situ Catalytic Pyrolysis of Algal Biomass in a Double Microfixed-Bed Reactor: Catalyst Deactivation and Its Coking Behavior, Energy and Fuels. 34 (2020) 1918–1928. https://doi.org/10.1021/ACS.ENERGYFUELS.9B04024/SUPPL_FILE/EF9B04024_SI_001.PDF.

[56] G. Abdulkareem-Alsultan, N. Asikin-Mijan, L.K. Obeas, R. Yunus, S.Z. Razali, A. Islam, Y. Hin Taufiq-Yap, In-situ operando and ex-situ study on light hydrocarbon-like-diesel and catalyst deactivation kinetic and mechanism study during deoxygenation of sludge oil, Chemical Engineering Journal. 429 (2022) 132206. https://doi.org/10.1016/J.CEJ.2021.132206.

[57] Y. Liu, F. Xu, N. Yuan, B. Lin, Y. Zhou, Revealing the Effect of Mass Transfer on Direct Dehydrogenation of Ethylbenzene Catalyzed by Phosphorous-doped Boron Nitride: Comparative Study, ChemCatChem. 14 (2022) e202101676. https://doi.org/10.1002/CCTC.202101676.

[58] A.T.D. Butland, R.J. Maddison, The specific heat of graphite: An evaluation of measurements, Journal of Nuclear Materials. 49 (1973) 45–56. https://doi.org/10.1016/0022-3115(73)90060-3.

[59] National Institute of Standards and Technology, Aluminium Oxide, United States Department of Commerce. (n.d.). https://webbook.nist.gov/cgi/cbook.cgi?ID=C1344281&Type=JANAFS&Plot=on (accessed March 27, 2022).

[60] E.E. (Ele E. Stansbury, R.A. (Robert A. Buchanan, Fundamentals of electrochemical corrosion, ASM International, 2000.

[61] J.H. Kwak, J.Z. Hu, D.H. Kim, J. Szanyi, C.H.F. Peden, Penta-coordinated Al3+ ions as preferential nucleation sites for BaO on γ-Al2O3: An ultra-high-magnetic field 27Al MAS NMR study, J Catal. 251 (2007) 189–194. https://doi.org/10.1016/J.JCAT.2007.06.029.

[62] K. Feng, R.E. Quevedo, J.T. Kohrt, M.S. Oderinde, U. Reilly, M.C. White, Late-stage oxidative C(sp3)–H methylation, Nature 2020 580:7805. 580 (2020) 621–627. https://doi.org/10.1038/S41586-020-2137-8.

[63] S. Dey, V. v. Praveen Kumar, The performance of highly active manganese oxide catalysts for ambient conditions carbon monoxide oxidation, Current Research in Green and Sustainable Chemistry. 3 (2020) 100012. https://doi.org/10.1016/J.CRGSC.2020.100012.

[64] Y. Xia, Y. Xiong, B. Lim, S.E. Skrabalak, Shape-Controlled Synthesis of Metal Nanocrystals: Simple Chemistry Meets Complex Physics?, Angewandte Chemie International Edition. 48 (2009) 60–103. https://doi.org/10.1002/ANIE.200802248.

[65] S. Dey, G.C. Dhal, D. Mohan, R. Prasad, The choice of precursors in the synthesizing of CuMnOx catalysts for maximizing CO oxidation, International Journal of Industrial Chemistry. 9 (2018) 199–214. https://doi.org/10.1007/S40090-018-0150-7/TABLES/10.

[66] Y. Mei, Q. Yang, H. Yang, J. Li, K. Zeng, Y. Chen, S. Zhang, H. Chen, Impact of cellulose deoxidization temperature on the composition of liquid products obtained by subsequent pyrolysis, Fuel Processing Technology. 184 (2019) 73–79. https://doi.org/10.1016/J.FUPROC.2018.11.003.

[67] C. Lang, X. Sécordel, A. Kiennemann, C. Courson, Water gas shift catalysts for hydrogen production from biomass steam gasification, Fuel Processing Technology. 156 (2017) 246–252. https://doi.org/10.1016/J.FUPROC.2016.09.004.

[68] I. Rossetti, · Antonio Tripodi, Catalytic Production of Renewable Hydrogen for Use in Fuel Cells: A Review Study, Topics in Catalysis 2022. 1 (2022) 1–20. https://doi.org/10.1007/S11244-022-01563-Z.

[69] P.M. Mortensen, J.D. Grunwaldt, P.A. Jensen, K.G. Knudsen, A.D. Jensen, A review of catalytic upgrading of bio-oil to engine fuels, Appl Catal A Gen. 407 (2011) 1–19. https://doi.org/10.1016/J.APCATA.2011.08.046.

[70] W. Schutyser, ab T. Renders, S. van den Bosch, S. Koelewijn, G.T. Beckham, B.F. Sels, Chemicals from lignin: an interplay of lignocellulose fractionation, depolymerisation, and upgrading, Chem. Soc. Rev. 47 (2018) 852. https://doi.org/10.1039/c7cs00566k.

[71] I. Kristianto, S.O. Limarta, H. Lee, J.M. Ha, D.J. Suh, J. Jae, Effective depolymerization of concentrated acid hydrolysis lignin using a carbon-supported ruthenium catalyst in ethanol/formic acid media, Bioresour Technol. 234 (2017) 424–431. https://doi.org/10.1016/J.BIORTECH.2017.03.070.

[72] A. Saraeian, M.W. Nolte, B.H. Shanks, Deoxygenation of biomass pyrolysis vapors: Improving clarity on the fate of carbon, Renewable and Sustainable Energy Reviews. 104 (2019) 262–280. https://doi.org/10.1016/J.RSER.2019.01.037.